Medium Effects on the Nucleation and Growth Mechanisms during the Redox Switching Dynamics of Conducting Polymers: Case of Poly(3,4-ethylenedioxythiophene)

Hyacinthe Randriamahazaka,*,† Thomas Bonnotte,† Vincent Noël,† Pascal Martin,† Jalal Ghilane,† Kinji Asaka,‡ and Jean-Christophe Lacroix†

Interfaces, Traitements, Organisation et Dynamique des Systèmes (ITODYS), CNRS-UMR 7086, Université Paris-Diderot, Bâtiment Lavoisier, 15 rue Jean-Antoine de Baïf, 75205 Paris Cedex 13, France, and Research Institute for Cell Engineering (RICE), AIST, Midorigaoka, Ikeda, Osaka 563-8577, Japan

Received: February 24, 2010

The redox switching dynamics of poly(3,4-ethylenedioxythiophene) (PEDOT) in an acetonitrile solution and a room temperature ionic liquid, 1-ethyl-3-methylimidazolium bis(trifluoromethylsulfonyl)imide (EmiTFSI), are investigated by means of potential step experiments. Redox switching can be viewed as a phase transition in which the nucleation and growth processes occur. We have developed a phenomenological model allowing the determination of the kinetic parameters. Two limiting cases are shown as follows: (i) a progressive and (ii) an instantaneous nucleation. In all cases, the growth process is described in terms of a self-exchange electron transfer reaction. We show that the mechanisms depend upon the medium. In acetonitrile, progressive nucleation and growth occur during oxidation (p-doping), whereas nucleation is instantaneous in the reduction of the PEDOT film. On the other hand, instantaneous nucleation and growth mechanisms are observed for both oxidation and reduction in EmiTFSI. The difference in the mechanisms results from the ionic exchange process associated with electron transfer and the initial structure of the film (open or compact). The influence of the applied potential on the dynamics is analyzed for both media.

1. Introduction

In the last 20 years, research on conjugated polymers has attracted considerable interest due to their applications in optical, electronic, and electromechanical devices.[1−5] In these devices, charge injection and transport mechanisms involving space and trapped charges have been studied intensively.[1,2] The possibility of electrochemical switching of these polymers from the insulating to the conducting state and vice versa makes their versatile applications possible. The rate of change of the desired properties, such as the electrical conductivity or the optical behavior, as a function of the experimental parameters, is of primary interest in most of these applications. The charge transport mechanisms in the conducting polymer involve not only electrons but also ions and solvent molecules.[6] Furthermore, the polymer configuration changes during the redox switching. Hillman and Bruckeinstein have stressed the importance of the film history and observation time scale on the redox switching.[7,8] Indeed, the initial and final states of the polymer depend upon the experimental conditions. These polymer states are not necessary in equilibrium. Also, the electrochemical switching involves multiple processes and many parallel paths.[7,8] Thus, the elucidation of the mechanisms responsible for such time-dependent properties is a difficult task. For an application point of view, a better understanding of the transport properties of mixed-conductivity materials, for instance, conducting polymers, is useful for improving the fabrication and operation of various electrochemical devices, such as solid-state batteries, electrochromic displays, sensors, and actuators.

The conducting polymer can be viewed as bicontinuous random networks of interpenetrating percolating phases composed by the solid, for instance, the polymer phase, and electrolyte solution, respectively. Also, the conducting polymers can be considered complex systems because these materials are disordered at the molecular scale and homogeneous at the macroscopic scale. In such systems, the dynamic processes include different length and time scales. Both fast and ultraslow molecular arrangements take place during the microscopic, mesoscopic, and macroscopic organization of the systems. Although the primary phenomenon is electron, ion, and solvent molecule transport,[6] the rate of charge transport during the oxidation step (p-doping) may depend upon the nucleation and the growth of conducting zones inside the neutral polymer[9−11] and also upon the compactness of the film.[12−14] Several authors have demonstrated that counterions played a major role in this conversion process.[15,16] Under certain experimental conditions, the rate-determining step of the overall process is ion transport. Moreover, the transition between the insulating and the conducting states is accompanied by a structural or conformational change.[12−14,17−19] This latter mechanism induces a volume change during the redox process. Also, a slow process occurs during the undoping process and determines the degree of compactness of the polymer. Hence, the relaxation processes can be described as the physicochemical changes in the polymer resulting from a perturbation, here mainly an electrical perturbation. In other words, the electrochemical history and the relaxation of the polymer film can affect the rate of the redox transformations.[12−14,20−25]

Several authors used the concept of a moving front to describe the redox switching of a conducting polymer. Aoki et al. have analyzed the effect of this moving front during the redox switching by using lattice models and percolation concepts.[24,26−31] Within the moving front concept, Lacroix et al. indicated that

* To whom correspondence should be addressed. Tel: 33(0)1 57 27 72 01. E-mail: hyacinthe.randria@univ-paris-diderot.fr.
† Université Paris-Diderot.
‡ Research Institute for Cell Engineering (RICE).

10.1021/jp1094432
Published on Web 12/21/2010

models based on pure diffusion processes were unable to explain the behavior of conducting polymers like polypyrrole.[32−34] These authors showed that it is necessary to consider a field-driven motion of ions in the description of ion transport during the redox switching of conducting polymers.[32−34] In the same way, Monte Carlo simulation indicated the predominant role played by migration in ion transport during this redox switching.[35,36] Otero et al. have proposed a model called electrochemical stimulated conformational relaxation (ESCR) in which two main processes were operative concerning the kinetics of the redox switching of conducting polymers.[12−14] First is the electrochemical (charging−discharging) process that includes the electronic and ionic charge transport. Second, this charging−discharging process initiates a conformational change of the polymer that may in turn affect the rate of the electrochemical reactions. In other words, the actual electrochemical processes are retarded due to the slowness of the relaxation of the polymer. The ESCR model has been successfully used to explain the conformational relaxation and the time-dependent conductivity of polypyrrole[12−14,37−40] and polyaniline films.[41] Also, the electrochemical behavior of an interpenetrating polymer network based on poly(3,4-ethylenedioxythiophene), PEDOT, has been analyzed within the framework of the ESCR model.[42] The first cycle or waiting time effects in the case of CV have been interpreted in terms of a slow configurational change of the polymer film and/or with the difficulty of removing the remaining charges from the insulating surroundings. However, an undoping sequence was not included in the ESCR model. Recently, Hillmann et al. studied the redox conversion and p-doping and n-doping processes of conducting polymers by means of an electrochemical quartz crystal microbalance.[43,44] These authors analyzed the electron/ion and solvent fluxes during redox conversion. They showed that the mechanisms depend upon the chemical nature of the solvent and ions.[45,46] In the case of electrochemical actuators, it has been reported that the chemical nature of the solvent and ions plays an important role.[47,48]

In the present work, the electrochemical responses of a conducting polymer-modified electrode in a monomer-free solution are studied to analyze the redox switching dynamics. We develop nucleation and growth models to describe the dynamics of the redox switching during the oxidation (p-doping) and reduction (undoping) processes of the conducting polymer. The nucleation phase may occur progressively or instantaneously. On the other hand, the growth process is described in terms of a bimolecular reaction or a self-exchange reaction, in which electron transfer occurs within an interface between undoped and p-doped polymer, as in the case of the moving front model.[34] During the growth process, electron transfer is coupled to counterion transport to maintain electroneutrality. This growth process may be limited by the electron transfer or counterion transport. As an example of conducting polymers, we have chosen PEDOT. Indeed, among the organic conducting polymers, PEDOT and its derivatives have attracted interest because they appear to be the most stable organic conducting polymers currently available.[49] Here, experimental data from chronocoulometry performed at different potentials are analyzed in terms of nucleation and growth mechanisms. The influence of the applied potential on the characteristic parameters is studied during both the oxidation and the reduction of the conducting polymer in acetonitrile (ACN) solution containing small anions, such as hexafluorophosphate, and in a room temperature ionic liquid (RTIL), 1-ethyl-3-methylimidazolium bis(trifluoromethylsulfonyl)imide (EmiTFSI). Previously, we have shown that no memory effect was observed in EmiTFSI.[50]

SCHEME 1: Nucleation and Growth Mechanisms during Redox Switching Dynamics of Conducting Polymers Where k_n and k_G Are the Nucleation and Growth Rate Constants, Respectively

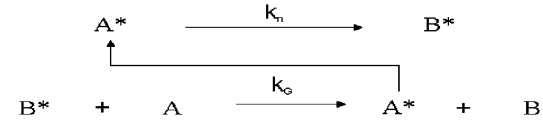

This absence of the memory effect will be of interest for the development of electrochemical actuators and electrochromic devices based on conducting polymers.

The proposed nucleation and growth mechanisms allowed us to rationalize the redox switching kinetics in various media. We pay special attention to the consequences of the chemical environments on the mechanisms involved. This work is motivated by the intrinsic physicochemical interest of the phenomena and by the attention that is being increasingly devoted to these materials with a view to applications. These issues will have strong implications for the design of microdevices, such as artificial muscles and electrochromic displays.[51,52]

2. Theoretical Model

We describe the charge transfer dynamics during the transition between the insulating (undoped) and the conducting states (p-doped), and vice versa, of PEDOT in terms of nucleation and growth mechanisms. Nucleation is connected to phase formation or transition. The electrochemical phase formation is accompanied by electron transfer processes. The heterogeneous nucleation depends on the number of available latently active centers (i.e., active surface sites), which can be transformed into real nuclei during the electrochemical phase formation. Here, the nuclei is described as a small fraction (or number) of the polymer phase involved in the nucleation process. The driving force of the nucleation can be varied simply by varying the applied potential. At the active sites, the nucleation probability depends upon the energetic favorable conditions. In the following, the latently active centers and real nuclei are called A^* and B^*, respectively. We assume that the number of active sites is several orders of magnitude below the number of possible sites at the electrode surface. To describe the oxidation and reduction processes by the same scheme, A and B describe the initial and final states, respectively.

Let us consider that the p-doping (or undoping) process follows the nucleation and growth mechanisms described as follows (Scheme 1). The nucleation process follows a first-order kinetics where k_n is the first-order nucleation rate constant associated with the heterogeneous electron transfer between the electrode surface and the polymer. In a real system, the active sites will follow a distribution of activation energies leading to a corresponding distribution of nucleation rates. For simplicity, we do not consider this aspect, and we assume that k_n does not vary during the nucleation and growth kinetics. The growth process is due to the self-exchange electron transfer between the oxidized and the reduced forms of the polymer and characterized a second-order growth rate constant k_G. According to Scheme 1, the nucleation and growth processes can be viewed as heterogeneous autocatalytic reactions. However, the nucleation and growth processes are limited because of energetic conditions that determine the probability of the nucleation.

The mass conservation equation can be expressed as

$$N_T = (n_{A^*})_t + (n_{B^*})_t + (n_A)_t + (n_B)_t \quad (1a)$$

$$N_T = N_t^* + (n_A)_t + (n_B)_t \quad (1b)$$

where $N^* = (n_{A^*})_t + (n_{B^*})_t$ is the quantity of the polymer involved in the nucleation process. In other words, N^* represents a finite number of latent nuclei at the beginning of the phase transition kinetics. We assume that N^* does not vary with time, but its value depends upon the experimental conditions (solvent, potential, etc.). As stated before, only a small part of the polymer participates in the nucleation process. Accordingly, one can write

$$N^* \ll (n_A)_t + (n_B)_t \quad (2)$$

Now, we introduce several dimensionless variables defined as

$$x_{B^*} = \frac{n_{B^*}}{N_T} \quad (3a)$$

$$x_{A^*} = \frac{n_{A^*}}{N_T} \quad (3b)$$

$$x_B = \frac{n_B}{N_T} \quad (3c)$$

$$x_A = \frac{n_A}{N_T} \quad (3d)$$

Also, we define a new dimensionless variable X_0 as

$$X_0 = x_{A^*} + x_{B^*} \quad (4)$$

where

$$X_0 \ll x_A + x_B \quad (5)$$

We consider that the nucleation process follows first-order kinetics

$$(x_{B^*})_t = X_0[1 - \exp(-k_n t)] \quad (6)$$

On the other hand, the growth process is described by a second-order (bimolecular) mechanism

$$\frac{-\mathrm{d}(x_A)_t}{\mathrm{d}t} = k_G(x_{B^*})_t(x_A)_t \quad (7)$$

At this stage, we can consider two limiting cases: (i) progressive nucleation and growth mechanisms (PNG) and (ii) instantaneous nucleation and growth mechanisms (ING) that we will analyze successively below.

2.1. PNGs. If the nucleation process is progressive, then a combination of eqs 6 and 7 gives

$$\frac{-\mathrm{d}(x_A)_t}{\mathrm{d}t} = k_G X_0[1 - \exp(-k_n t)] \times (x_A)_t \quad (8a)$$

Then

$$\frac{-\mathrm{d}(x_A)_t}{(x_A)_t} = k_G X_0[1 - \exp(-k_n t)] \times \mathrm{d}t \quad (8b)$$

By integrating eq 8a, one obtains

$$-\ln\left[\frac{(x_A)_t}{(x_A)_{t=0}}\right] = k_G X_0 t - \frac{k_G X_0}{k_n}[1 - \exp(-k_n t)] \quad (9)$$

Thus

$$(x_A)_t = (x_A)_{t=0} \times \exp\left\{-k_G X_0 t + \frac{k_G X_0}{k_n}[1 - \exp(-k_n t)]\right\} \quad (10)$$

According to the boundary conditions—eqs 1a, 2, and 4—one can write

$$(x_B)_t \approx 1 - (x_A)_t \quad (11)$$

and

$$(x_A)_{t=0} \approx 1 \quad (12)$$

Then, we obtain

$$(x_B)_t = 1 - \exp\left\{-k_G X_0 t + \frac{k_g X_0}{k_n}[1 - \exp(-k_n t)]\right\} \quad (13)$$

By using Faraday' law, the charge consumed Q_t during the formation of B from A is

$$Q_t = Q_T\left\{1 - \exp\left[-k_G X_0 t + \frac{k_G X_0}{k_n}(1 - \exp(-k_n t))\right]\right\} \quad (14)$$

where Q_T is total charge at the end of the growth process.

At this stage, it is of interest to compare eq 14 with the equation describing the two-dimensional nucleation according to an exponential law with diffusion-controlled growth.[53] Indeed, in the case where the growing centers are cylindrical and if the rate of advance of the radius r is controlled by symmetrical hemicylindrical diffusion about an axis at right angles to the two-dimensional nucleus (surface diffusion-controlled growth), the time dependence of the radius is given by

$$r = K(Dt)^{1/2} \quad (15)$$

where K is a constant that depends on potential and D is the diffusion coefficient. In addition, it will be assumed that one-step nucleation takes place according to an exponential law. If nucleation and growth occur simultaneously, the resulting change in the surface coverage θ_t with time is

$$\theta'_t = \int_0^t f(u)\left(\frac{dN}{dt}\right)_{t=(t-u)} du \quad (16a)$$

where $f(u)$ is the growth law describing the change in the surface coverage of a single center, N is the number of centers, and u is the age of the center. One has[53]

$$\theta'_t = K_Z\{1 - \exp(-k_n t)\} \quad (16b)$$

where K_Z is a constant including the maximum number of nuclei and k_n is the nucleation rate constant.

It is well-known that an overlap of growth centers occurs during the growth process. The overlap between neighboring centers is usually taken into account by applying the Avrami theorem.[54] It considered a new phase nucleated by germ nuclei (equivalent to active sites), having a number density N. The number of actual germ nuclei decreases in two ways: (i) through becoming active growth nuclei and (ii) by being swallowed by another nearby growing nucleus.[54] Accordingly, the fraction θ_t of the new phase that is generated from a two-dimensional nucleation according to an exponential law with diffusion-controlled growth is given as[53]

$$\theta_t = 1 - \exp\left\{-K_Z t + \frac{K_Z}{k_n}[1 - \exp(-k_n t)]\right\} \quad (17)$$

Now, it is of interest to compare eqs 13 and 17. As shown before, eq 17 described a two-dimensional nucleation according to an exponential law with diffusion-controlled growth. However, it is well-known that the dimensionality of the electrochemical phase formation (2D vs 3D) for conducting polymer varies during the nucleation and growth processes because of the conformational and volume changes.[7,8,12−14] This fact explains why we use the fraction of new phase formed in eq 13. By comparing eqs 13 and 17, we show that these equations have the same mathematical form. This behavior indicates that the two approaches are equivalent despite the fact that the geometrical aspects are not taken into account in the present work.

2.2. INGs. Now, let us consider the other limiting case. The nucleation process is considered to be instantaneous if

$$k_n t \gg 1 \quad (18)$$

then

$$x_{B^*} \approx X_0 \quad (19)$$

In this case, eq 7 can be rewritten as

$$\frac{-d(x_A)_t}{dt} = k_G X_0 (x_A)_t \quad (20)$$

One obtains

$$\frac{-d(x_A)_t}{(x_A)_t} = k_G X_0\, dt \quad (21)$$

By integrating eq 21, one has

$$(x_A)_t = (x_A)_{t=0} \times \exp(-k_G X_0 t) \quad (22)$$

According to the boundary conditions, one can write

$$(x_B)_t = 1 - \exp(-k_G X_0 t) \quad (23)$$

By using Faraday's law, the charge consumed Q_t during the formation of B from A is

$$Q_t = Q_T\{1 - \exp(-k_G X_0 t)\} \quad (24)$$

This last equation—eq 24—allows us to determine the amount of PEDOT transformed from the initial to the final state during the oxidation (reduction) process for INGs.

3. Experimental Section

The monomer 3,4-ethylenedioxythiophene (EDOT) was kindly provided by Bayer AG and distilled prior to use. The background electrolyte for the electrodeposition of PEDOT was $LiClO_4$ supplied by Fluka. ACN (HPLC grade) and tetrabutyl ammonium hexafluorophosphate (NBu_4PF_6) were from Acros. The RTIL EmiTFSI was synthesized according to published procedures.[55]

The electrochemical experiments were carried out with a three-compartment three-electrode glass cell. The working electrode was a Pt disk (2.0 mm radius), and a Pt wire was used as the counterelectrode. The reference electrode was an Ag|AgCl electrode for ACN. It was calibrated with the ferricinium/ferrocene/ (Fc^+|Fc) couple in ACN (= 400 mV vs Ag|AgCl). In this report, all potentials are referenced to the Fc^+|Fc couple. Electrochemical experiments [cyclic voltammetry (CV) and chronocoulometry] were performed on a CHI 660B electrochemical analyzer workstation (CH Instruments, Austin, TX). The working electrode was polished carefully with alumina slurry and cleaned in an ultrasonic bath before each experiment. Prior to all experiments, the solutions were purged with argon, and an argon atmosphere was maintained over the solution during the measurements.

PEDOT was electrodeposited on the electrode surface from a solution of the monomer in ACN, as described in previous work.[56] Electropolymerization was achieved by a second step to 1 V vs Fc^+|Fc for 15 s in an ACN containing 2×10^{-2} M EDOT. The polymerization charge was 8 mC. On the basis of our previous works, the film thickness was estimated as 0.25 μm by assuming that the electrodeposition charge efficiency was 100% and gave 7.90 ± 0.05 μm/(C cm^{-2}).[56,57] After the electrodeposition, the modified electrode was washed with ACN. To ensure complete replacement of the deposition electrolyte by the characterization solution, the modified electrodes were redox cycled at least 10 times after solution exchange. The effectiveness of this conditioning procedure was demonstrated by the reproducibility of the CV responses.

The chronoamperometry and chronocoulometry experiments were carried out in deaerated 0.1 M NBu_4PF_6 in ACN and in EmiTFSI. Each measurement was repeated three times. Experients were carried out at room temperature (18 ± 2 °C). The repeatability and the reproductibility of experiments are established, such that the coefficient of variation is lower than 10%. Experimental data were fitted with nonlinear least-squares methods (NLLS) by using the Marquardt−Levenberg algorithm as available in the Origin Software (Microcal, Northampon, MA). The experimental charge−time curves were fitted with

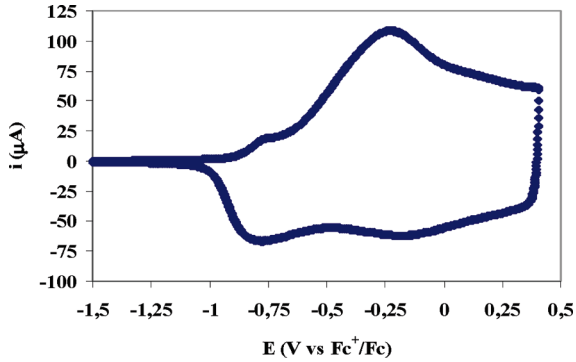

Figure 1. Cyclic voltammogram of PEDOT-modified electrode in 0.1 M NBu_4PF_6 in ACN: scan rate = 0.1 V s^{-1}. The film thickness is 0.25 μm.

the theoretical functions corresponding to the above models (PGN and ING mechanisms), and the best model was indicated based on the statistical measures of the NLLS fittings (i.e., σ, the variance; and/or R^2, the correlation coefficient). A minimum of 50 iterations (or more) was performed until the fractional change in the χ^2 value was within the tolerance limit, which was set to 0.0005. Usually, a value on the order of 10^{-4} of the fractional χ^2 change was obtained in the final iterations.

4. Results

4.1. Electrochemical Responses in NBu_4PF_6 + ACN. Figure 1 shows a typical CV of a PEDOT-modified electrode in a monomer-free solution of NBu_4PF_6 in ACN at a scan rate of 0.1 V/s. The CV displays an anodic prepeak at −0.75 V and a peak current at 0.23 V followed by a plateau current. The reverse scan shows two peaks at −0.16 and −0.78 V. These results are in agreement with published results.[25,43] The peak current varies linearly with the scan rate (scan rates ranging from 0.005 to 0.2 V/s) and indicates thin-layer behavior.

To study the dynamics of redox switching, we perform potential step experiments during the oxidation and reduction. For oxidation and reduction, the initial potentials were set at −1.2 and 0.6 V, respectively. Typical chronoamperograms (CA) are shown in Figure 2. The shapes of the CA curves during the oxidation and reduction differ radically. This indicates that the mechanisms do not follow the same path. Also, if we look at the CV in Figure 1, we also observe that the reverse scan (reduction) is not the mirror of the forward scan (oxidation). In other words, the transformation (oxidation/reduction) of PEDOT during redox switching is an irreversible process from a thermodynamic point of view. Because the main goal of this work is the analysis of the nucleation and growth mechanisms, we shall study the oxidation and reduction processes separately.

The time dependence of the charge variation during oxidation in ACN solution is shown Figure 3. We find that these curves can be analyzed with the following equation

$$Q_{ox,tot}(t) = Q_{ox,t_\infty}^{open}\left\{1 - \exp\left[-k_{G-ox}^{open}\cdot X_0^{open}\cdot t + \frac{k_{G-ox}^{open}\cdot X_0^{open}}{k_{ox,n}} \times (1 - \exp(-k_{ox,n}\cdot t))\right]\right\} + Q_{ox,t_\infty}^{comp}\cdot\{1 - \exp(-k_{G-ox}^{comp}\cdot X_0^{comp} t)\} \quad (25)$$

where $Q_{ox,tot}$ is the overall charge at instant t during the oxidation, Q_{ox,t_∞}^{open} is the total charge for the open part of the film, k_{G-ox}^{open} and X_0^{open} are the growth rate constant and the fraction of the open polymer structure involved in the nucleation process, $k_{ox,n}$ is the nucleation rate constant, Q_{ox,t_∞}^{comp} is the total charge for the compact part of the film, and k_{G-ox}^{comp} and X_0^{comp} are the growth rate constant and the fraction of the compact polymer structure involved in the nucleation process. The first term of eq 25 describes progressive nucleation and growth of the open structure of the film, called the $(PNG)_o$ mechanism. The second part of eq 25 characterizes instantaneous nucleation and growth of the compact structure of the film, called the $(ING)_c$ mechanism. In the following, for simplicity, the oxidation of PEDOT in ACN during the potential step experiment is termed $(PNG)_o$-$(ING)_c$. Also, eq 25 can be rewritten as

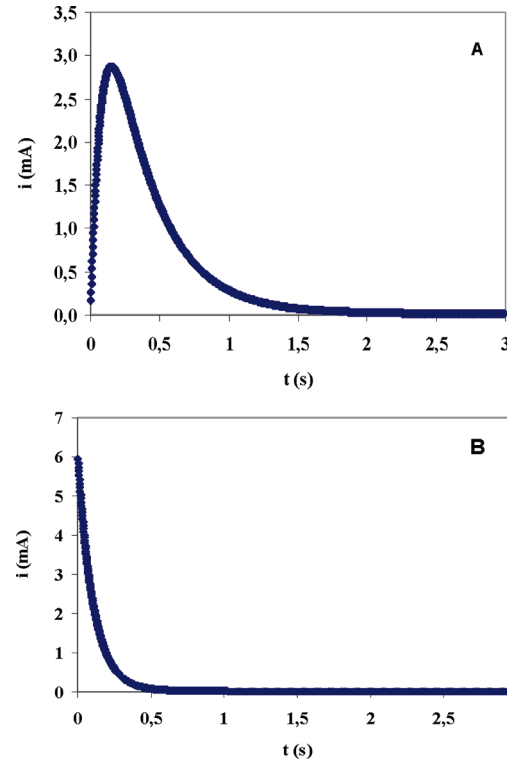

Figure 2. Chronoamperograms during the oxidation (A) and reduction (B) of PEDOT-modified electrode in 0.1 M NBu_4PF_6 in ACN. The oxidation reaction is performed by a potential step form −1.2 to 0.0 V vs Fc^+ | Fc. For the reduction reaction, the potential step is form 0.6 to −0.5 V vs Fc^+ | Fc.

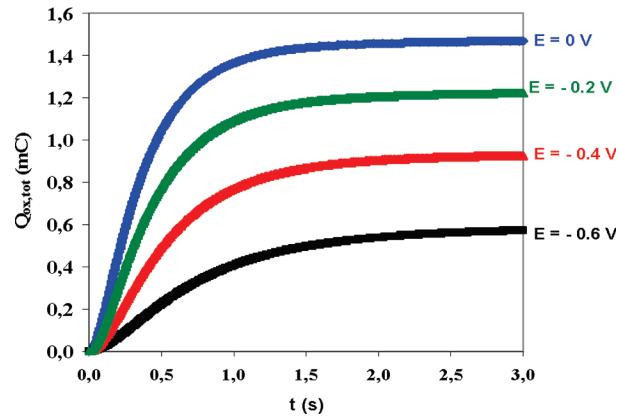

Figure 3. Variation of anodic charge $Q_{ox\text{-}tot}$ as a function of time for PEDOT-modified electrode in 0.1 M NBu_4PF_6 in ACN. The initial potential is −1.2 V vs Fc^+ | Fc; the final potentials are indicated in the figure.

$$Q_{ox,tot}(t) = Q_{ox,t_\infty}^{open}\left\{1 - \exp\left[-k_{G-ox}^{open*}t + \frac{k_{G-ox}^{open*}}{k_{ox,n}}(1 - \exp(-k_{ox,n}t))\right]\right\} + Q_{ox,t_\infty}^{comp}\{1 - \exp(-k_{G-ox}^{comp*}t)\} \quad (26)$$

where

$$k_{G-ox}^{open*} = k_{G-ox}^{open} \cdot X_0^{open} \quad (27)$$

and

$$k_{G-ox}^{comp*} = k_{G-ox}^{comp} \cdot X_0^{comp} \quad (28)$$

The PEDOT film deposited onto the electrode surface can be viewed as interpenetrating networks combining a solid phase, for instance, the polymer, and a liquid phase containing the electrolyte solution. We have shown in previous work that this film contains two types of coexisting zones: compact and open structures.[57,58] These zones display different characteristics from the thermodynamic and kinetic points of view. Our previous work indicates that the electrochemical impedance spectroscopy results fit well an impedance circuit containing two parallel paths.[58] Then, the existence of these coexisting zones is taken into account during the relaxation kinetics. Here, we show that eq 25 or 26 allows us to fit the experimental data and to determine the feature parameters of the oxidation of PEDOT. In all cases, we obtain excellent fits with correlation coefficients higher than 0.99.

Now, we can examine the influence of the applied potential E_{app} on the characteristic kinetic parameters. According to eq 26, the oxidation process is characterized by $k_{ox,n}$, k_{G-ox}^{open*}, Q_{ox,t_∞}^{open}, k_{G-ox}^{comp*}, and Q_{ox,t_∞}^{comp}. As shown in Figure 4, $k_{ox,n}$ increases linearly with E_{app}. This trend indicates that the nucleation process is potential-dependent. Also, we observe a threshold potential E_{ox}^* of −1.020 V. A nonlinear increase in k_{G-ox}^{open*} with E_{app} and a linear variation of Q_{ox,t_∞}^{open} with E_{app} are observed in Figure 5. The linear variation of Q_{ox,t_∞}^{open} vs E_{app} shows the capacitive property of the modified electrode. Furthermore, Q_{ox,t_∞}^{open} has the same threshold potential E_{ox}^*, of −1.020 V, as in the case of $k_{ox,n}$ (Figure 4). This behavior indicates clearly a correlation between the nucleation (via $k_{ox,n}$) and the growth processes (viaQ_{ox,t_∞}^{open}) for the open structure of the film. For the compact zone, the variations of k_{G-ox}^{comp*} and Q_{ox,t_∞}^{comp} as a function of the applied potential E_{app} are reported in Figure 6. An increase in k_{G-ox}^{comp*}

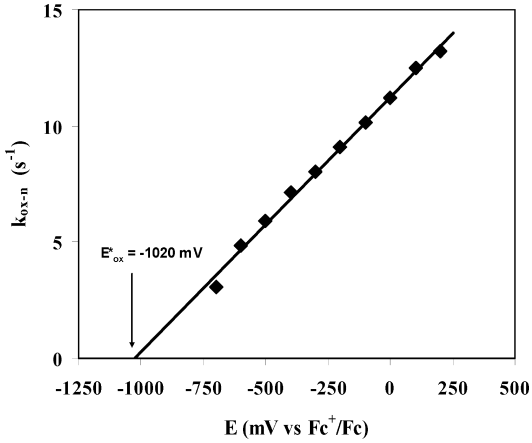

Figure 4. Variation of nucleation rate constant $k_{ox,n}$ as a function of the applied potential E_{app} during oxidation of PEDOT-modified electrode in 0.1 M NBu_4PF_6 in ACN.

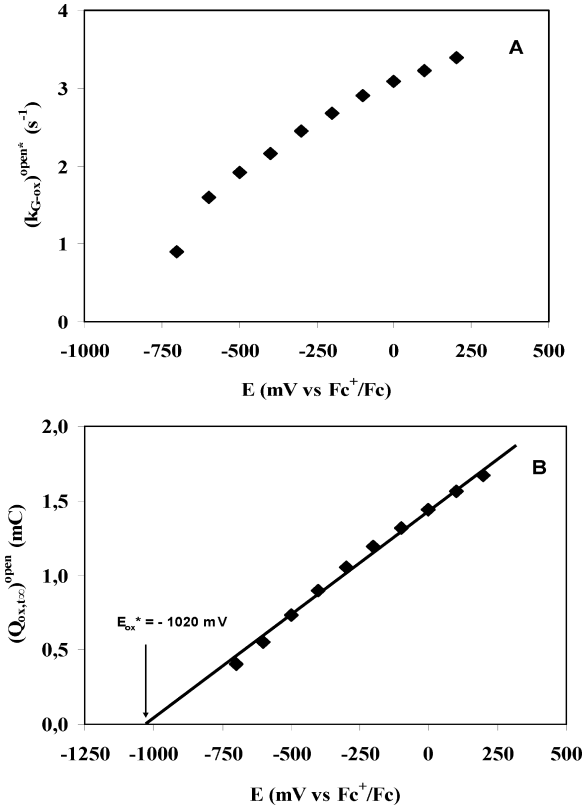

Figure 5. Variation of growth rate constant k_{G-ox}^{open*} (A) and the anodic charge Q_{ox,t_∞}^{open} (B) for the open state as a function of the applied potential E_{app} during oxidation of PEDOT-modified electrode in 0.1 M NBu_4PF_6 in ACN.

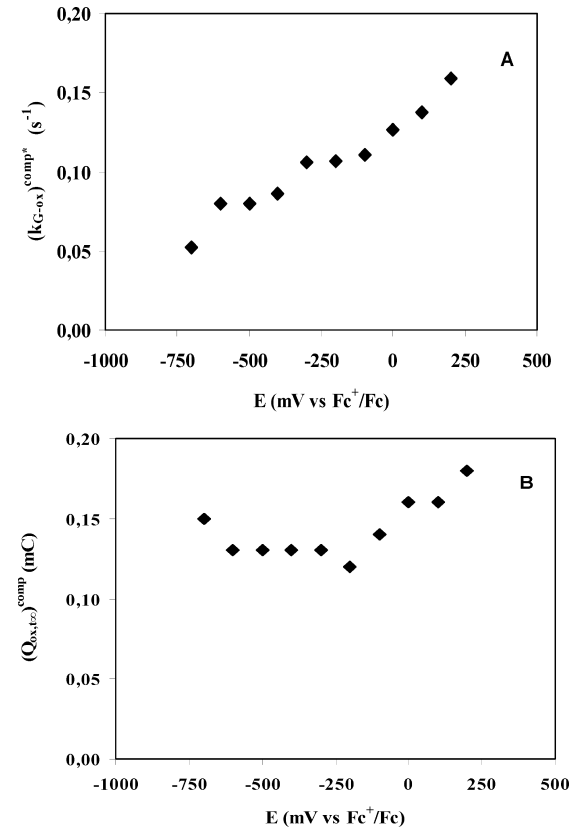

Figure 6. Variation of growth rate constant k_{G-ox}^{comp*} (A) and the anodic charge Q_{ox,t_∞}^{comp} (B) for compact state as a function of applied potential E_{app} during oxidation of PEDOT-modified electrode in 0.1 M NBu_4PF_6 in ACN.

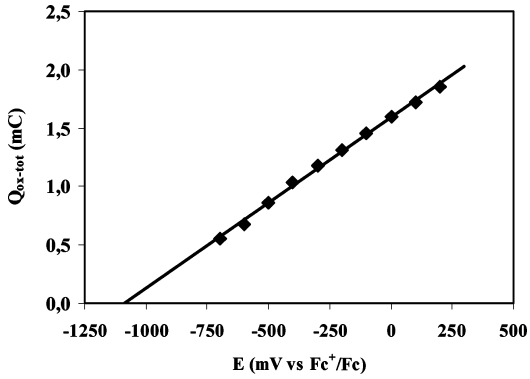

Figure 7. Variation of the total anodic charge $Q_{ox,tot}$ as a function of applied potential E_{app} during oxidation of PEDOT-modified electrode in 0.1 M NBu_4PF_6 in ACN.

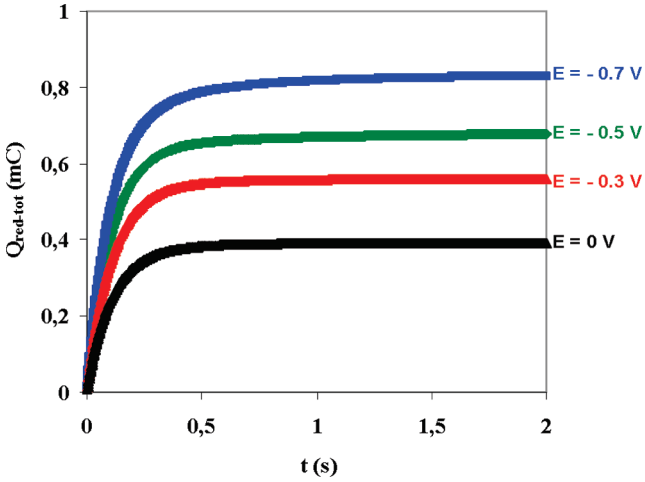

Figure 8. Variation of cathodic charge $Q_{red,tot}$ as a function of time for PEDOT-modified electrode in 0.1 M NBu_4PF_6 in ACN. The initial potential is 0.6 V; final potentials are indicated in the figure.

with E_{app} is observed. However, the variation of Q_{ox,t_∞}^{comp} as a function of E_{app} displays a minimum that is located in the potential range where the prepeak current during the oxidation of PEDOT occurs in ACN + NBu_4PF_6, as shown in Figure 1. It should be noted that for all potentials, Q_{ox,t_∞}^{open} is much higher than Q_{ox,t_∞}^{comp}. Then, the total charge $Q_{ox,tot}$ ($= Q_{ox,t_\infty}^{open} + Q_{ox,t_\infty}^{comp}$) varies linearly with E_{app} (Figure 7), as in the case of Q_{ox,t_∞}^{open}. To quantify the relative contribution of the open zone during the switching kinetics, the ratio R_{ox} of Q_{ox,t_∞}^{open} with respect to $Q_{ox,tot}$ is determined. We show a slight increase in R_{ox} with E_{app} followed by a plateau (see the Supporting Information, Figure S1).

After examining the oxidation process, we can now study the reduction. Here, we speak about the reduction of a preoxidized PEDOT film. In this sense, the term reduction does not refer to an n-doping process. The time dependence of the charge variation is shown Figure 8. We find that this process can be analyzed by the following equation

$$Q_{red,tot}(t) = Q_{red,t_\infty}^{open}\{1 - \exp(-k_{G-red}^{open} \cdot X_0^{open} t)\} + Q_{red,t_\infty}^{comp}\{1 - \exp(-k_{G-red}^{comp} \cdot X_0^{comp} t)\} \quad (29)$$

where $Q_{red,tot}$ is the overall charge at instant t during the reduction, Q_{red,t_∞}^{open} and k_{G-red}^{open} are the total charge and the growth rate constant for the open part of the film, respectively, X_0^{open} is the fraction of the open polymer structure involving to the nucleation process, Q_{red,t_∞}^{comp} and k_{G-red}^{comp} are the total charge and

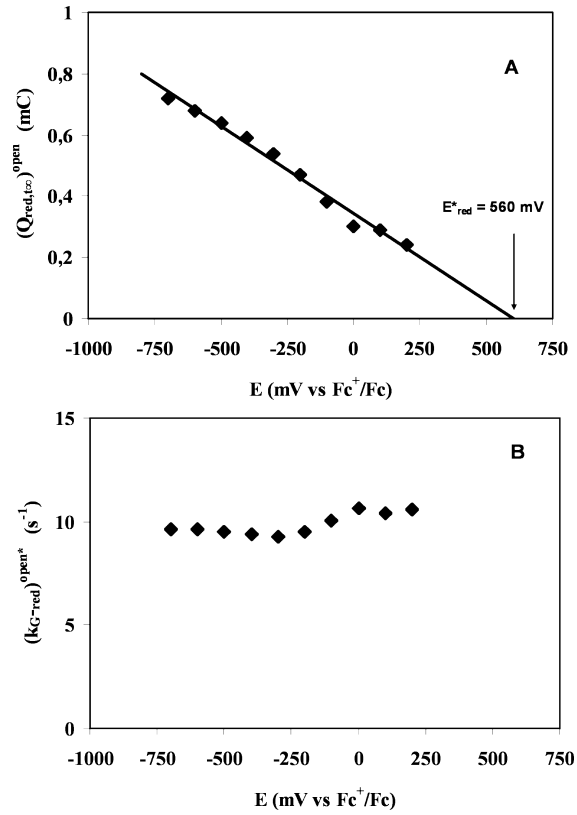

Figure 9. Variation of cathodic charge Q_{red,t_∞}^{open} (A) and the growth rate constant k_{G-red}^{open*} (B) for open state as a function of applied potential E_{app} during reduction of PEDOT-modified electrode in 0.1 M NBu_4PF_6 in ACN.

the growth rate constant for the compact part of the film, respectively, and X_0^{comp} is the fraction of the compact polymer structure involved in the nucleation process. The first term of eq 29 describes an instantaneous nucleation and growth of the open structure of the film, called the $(ING)_o$ mechanism. The second part of eq 29 characterizes instantaneous nucleation and growth of the compact structure of the film, called the $(ING)_c$ mechanism. In the following, the reduction of PEDOT in ACN during the potential step experiment is termed $(ING)_o$-$(ING)_c$. Then, eq 29 can be rewritten as

$$Q_{red,tot}(t) = Q_{red,t_\infty}^{open}\{1 - \exp(-k_{G-red}^{open*} \cdot t)\} + Q_{red,t_\infty}^{comp}\{1 - \exp(-k_{G-red}^{comp*} \cdot t)\} \quad (30)$$

where

$$k_{G-red}^{open*} = k_{G-red}^{open} \cdot X_0^{open} \quad (31)$$

and

$$k_{G-red}^{comp*} = k_{G-red}^{comp*} X_0^{comp} \quad (32)$$

As shown in Figure 9, Q_{red,t_∞}^{open} varies linearly with the applied potential E_{app}. A threshold potential E_{red}^* of 0.56 V is observed for the reduction process. However, the apparent growth rate constant k_{G-red}^{open*} does not vary notably with E_{app}. For the compact structure of the film, the variations of both Q_{red,t_∞}^{comp} and k_{G-red}^{comp*} with E_{app} are shown in Figure 10. One observes that k_{G-red}^{comp*}

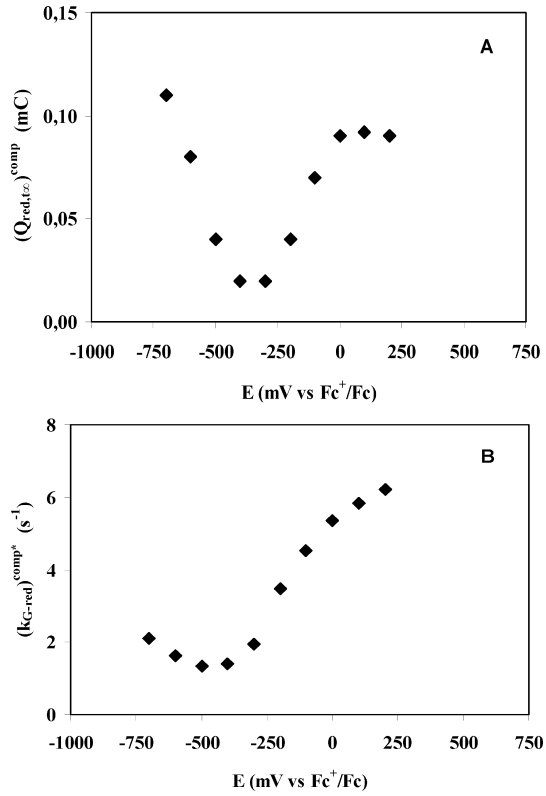

Figure 10. Variation of the cathodic charge Q_{red,t_∞}^{comp} (A) and the growth rate constant k_{G-red}^{comp*} (B) for compact state as a function of applied potential E_{app} during reduction of PEDOT-modified electrode in 0.1 M NBu_4PF_6 in ACN.

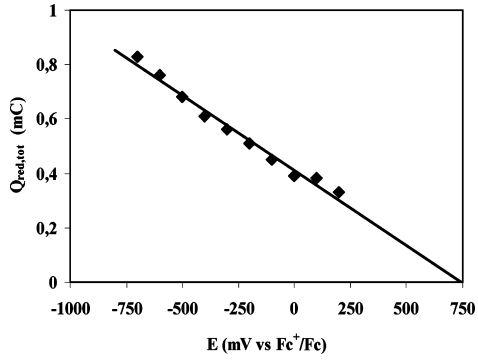

Figure 11. Variation of total cathodic charge $Q_{red,tot}$ as a function of applied potential E_{app} during reduction of PEDOT-modified electrode in 0.1 M NBu_4PF_6 in ACN.

displays a minimum around −0.5 V. In all cases, Q_{red,t_∞}^{comp} is lower than Q_{red,t_∞}^{open}. Accordingly, the total charge for the reduction $Q_{red,tot}$ ($= Q_{red,t_\infty}^{open} + Q_{red,t_\infty}^{comp}$) varies linearly with E_{app} (Figure 11), as in the case of Q_{red,t_∞}^{open}. The ratio of Q_{red,t_∞}^{open} with respect to $Q_{red,tot}$ displays a maximum at a potential around −0.400 V (see the Supporting Information, Figure S2). Also, k_{G-red}^{comp*} is lower that $k_{G-red,O}^{*}$, as shown in Figures 9 and 10.

4.2. Electrochemical Responses in 1-Ethyl-3-methylimidazolium Bis(trifluoromethyl-sulfonyl)imide. The typical CV of a PEDOT-modified electrode in EmiTFSI is shown in Figure 12. We perform the same procedure as in the previous section, for instance, a series of potential steps. The chronocoulograms for the oxidation and reduction of the electrode in EmiTFSI are shown in Figures 13 and 14. In all cases, there is a rapid increase in the charge during the initial stage followed by a

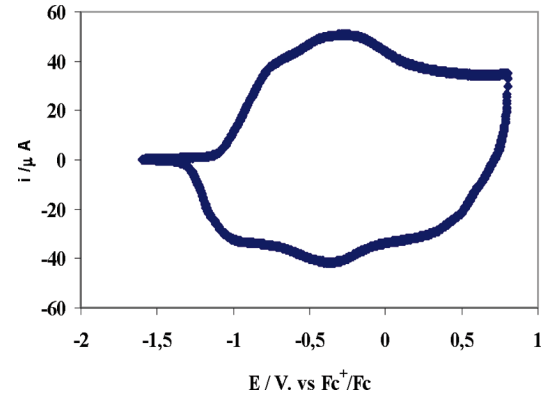

Figure 12. Cyclic voltammogram of PEDOT-modified electrode in EmiTFSI; scan rate = 0.1 V s^{-1}. The film thickness is 0.25 μm.

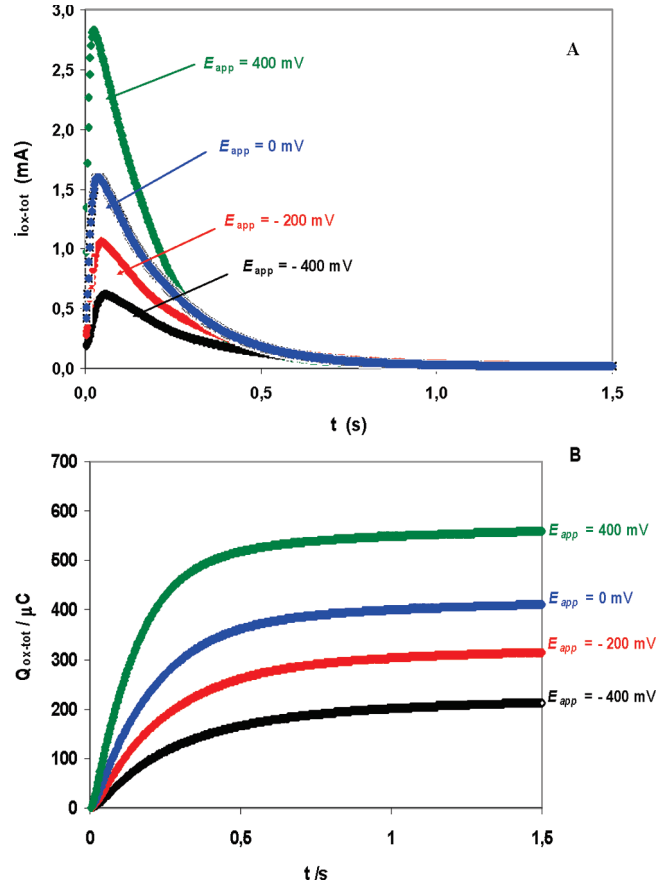

Figure 13. Variation of anodic current $i_{ox,tot}$ (A) and charge $Q_{ox,tot}$ (B) as a function of time for PEDOT-modified electrode in EmiTFSI. The initial potential is −1.2 V vs Fc^+ | Fc; final potentials are indicated in the figure.

slow variation. The time dependence of the charge during the oxidation and reduction can be described as follows

$$Q_{ox,tot}(t) = Q_{ox,t_\infty}^{open}\{1 - \exp(-k_{G-ox}^{open*} \cdot t)\} + Q_{ox,t_\infty}^{comp}\{1 - \exp(-k_{G-ox}^{comp*} \cdot t)\} \quad (33)$$

and

$$Q_{red,tot}(t) = Q_{red,t_\infty}^{open}\{1 - \exp(-k_{G-red}^{open*} \cdot t)\} + Q_{red,t_\infty}^{comp}\{1 - \exp(-k_{G-red}^{comp*} \cdot t)\} \quad (34)$$

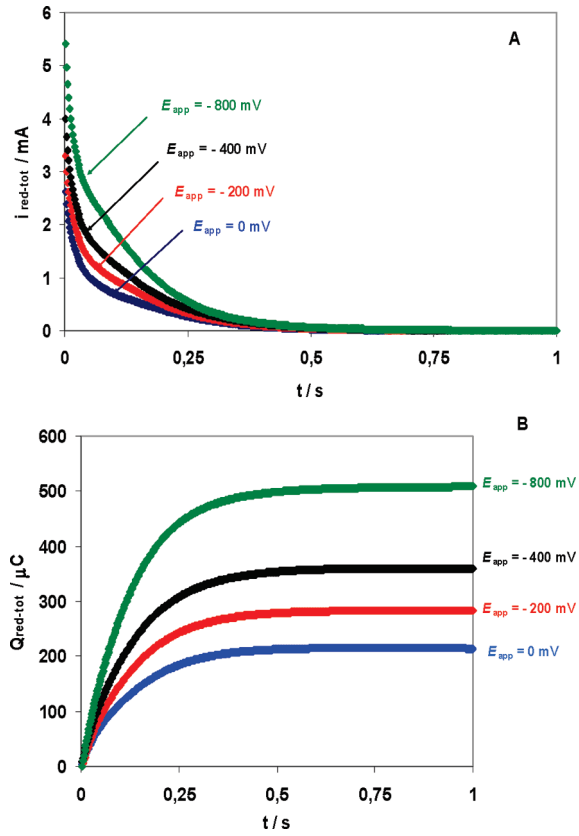

Figure 14. Variation of cathodic current $i_{red,tot}$ (A) and charge $Q_{red,tot}$ (B) as a function of time for PEDOT-modified electrode in EmiTFSI. The initial potential is 0.6 V vs Fc^+ | Fc; final potentials are indicated in the figure.

with

$$k_{G-ox}^{open*} = k_{G-ox}^{open} \cdot X_0^{open} \quad (35)$$

$$k_{G-ox}^{comp*} = k_{G-ox}^{comp} \cdot X_0^{comp} \quad (36)$$

$$k_{G-red}^{open*} = k_{G-red}^{open} \cdot X_0^{open} \quad (37)$$

and

$$k_{G-red}^{comp*} = k_{G-red}^{comp} \cdot X_0^{comp} \quad (38)$$

where $Q_{ox,tot}$ ($Q_{red,tot}$) is the overall charge at instant t for the oxidation (reduction), Q_{ox,t_∞}^{open} (Q_{red,t_∞}^{open}) is the total charge and k_{G-ox}^{open*}(k_{G-red}^{open*}) is the growth rate constant for the open part of the film, X_0^{open} is the fraction of the open polymer structure involving to the nucleation process, Q_{ox,t_∞}^{comp} (Q_{red,t_∞}^{comp}) is the total charge for the compact part of the film, k_{G-ox}^{comp*} (k_{G-red}^{comp*}) is the growth rate constant, and X_0^{comp} is the fraction of the compact polymer structure involved in the nucleation process. The first term of eq 33 (eq 34) describes instantaneous nucleation and growth of the open structure of the film, the $(ING)_o$ mechanism. The second part of eq 33 (eq 34) characterizes instantaneous nucleation and growth of the compact structure of the film, the $(ING)_c$ mechanism. Then, the oxidation and reduction of PEDOT in EmiTFSI during the potential step experiment are called $(ING)_o$-$(ING)_c$. These equations (eqs 33 and 34) allow us to fit the experimental data and to determine the feature parameters

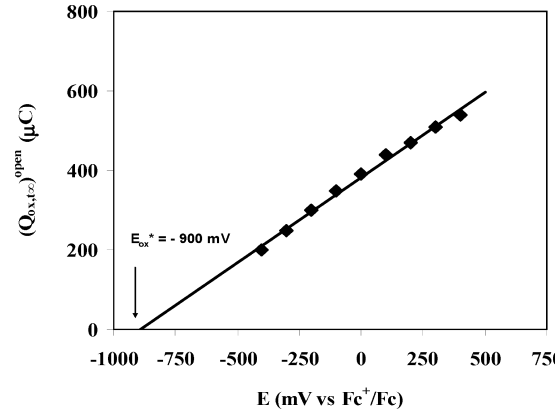

Figure 15. Variation of anodic charge Q_{ox,t_∞}^{open} for open state as a function of applied potential E_{app} during oxidation of PEDOT-modified electrode in EmiTFSI.

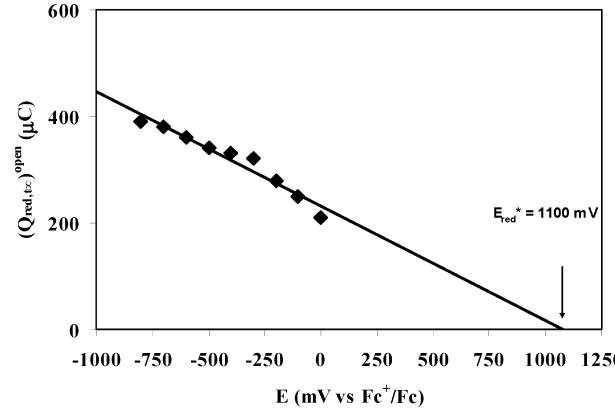

Figure 16. Variation of cathodic charge Q_{red,t_∞}^{open} for open state as a function of the applied potential E_{app} during the reduction of PEDOT-modified electrode in EmiTFSI.

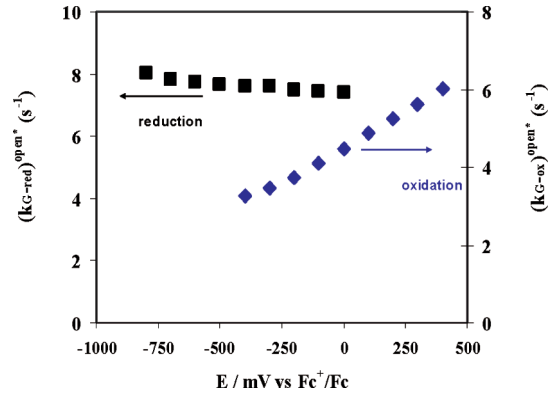

Figure 17. Variation of growth rate constant k_{G-ox}^{open*} (oxidation) and k_{G-red}^{open*} (reduction) as a function of applied potential E_{app}, for open state, during redox switching of PEDOT-modified electrode in EmiTFSI.

of the redox switching of PEDOT in EmiTFSI. In all cases, we obtain excellent fits with correlation coefficients higher than 0.99.

As shown in Figures 15 and 16, the maximal charge for both oxidation and reduction, Q_{ox,t_∞}^{open} and Q_{red,t_∞}^{open}, vary linearly with the applied potential E_{app} and displays threshold potentials E_{ox}^* and E_{red}^* of −0.9 and 1.1 V, respectively. The variations of the growth rate constant k_{G-ox}^{open*} and k_{G-red}^{open*} as a function of the applied potential E_{app} are shown in Figure 17. One observes that k_{G-red}^{open*} decreases slowly with E_{app}. On the other hand, an increase of k_{G-ox}^{open*} with E_{app} is shown. The variations of the total charge $Q_{red,tot}$ and $Q_{ox,tot}$ as a function of the applied potential E_{app} are reported

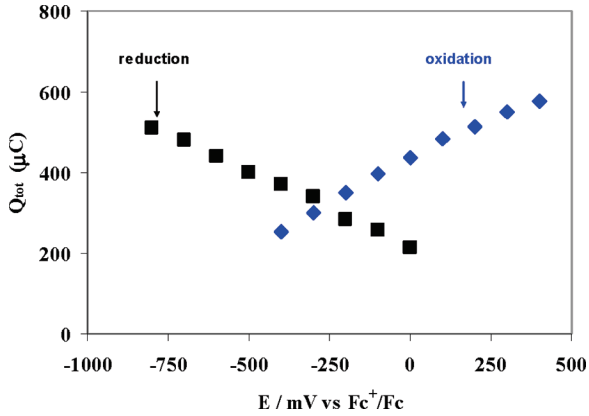

Figure 18. Variations of total charge $Q_{red,tot}$ (reduction) and $Q_{ox,tot}$ (oxidation) as a function of applied potential E_{app} for PEDOT-modified electrode in EmiTFSI.

in Figure 18. Also, we observe that both Q_{ox,t_∞}^{comp} and Q_{red,t_∞}^{comp} are lower than Q_{ox,t_∞}^{open} and Q_{red,t_∞}^{open}, respectively. The ratios of Q_{red,t_∞}^{open} with respect to $Q_{red,tot}$ and of Q_{ox,t_∞}^{open} with respect to $Q_{ox,tot}$ increase with E_{app} (see the Supporting Information, Figure S3). These results indicate clearly that the major part in the charge involves the open state of the film during the redox switching in EmiTFSI.

5. Discussion

In the interpretation of the chronoamperometry or chronocoulometry data, it is appropriate to have mechanistic support relating the transformation of PEDOT between the neutral (undoped) and the oxidized (doped) states. Here, we take into account both the phase transformation kinetics (nucleation and growth processes) and the influence of the initial polymer structure before the transformation (open and compact states). However, we do not consider the geometrical shape of the nuclei involved in the nucleation process because the polymer film displays a complex structure. Previously, we have shown that the PEDOT film deposited onto the electrode surface had a fractal-like feature.[59] Then, we use directly Faraday law to follow the redox transformation. Here, we study the redox switching dynamics in two media. First, in NBu_4PF_6 + ACN, anion exchange is the main path for maintaining the electroneutrality of the system.[4143] In this case, the anion transfer controls the redox switching kinetics. On the other hand, when the redox transformation is carried out in a RTIL, EmiTFSI, then a cation is exchanged.[60] In the latter case, the cation transport is the rate limiting step. Thus, experimental conditions under which permselectivity occurs allow us to investigate the influence of the medium on the redox transformation processes.

According to these data, we show that the mechanisms depend greatly on the chemical environment. We show that in NBu_4PF_6 + ACN, $(PNG)_o$-$(ING)_c$ mechanisms occur during the oxidation, whereas $(ING)_o$-$(ING)_c$ are observed during the reduction. Because anion uptake takes place during oxidation, then a conformational change inducing an increase in the film volume is expected.[7,8,12,13] This increase in volume should be the rate-limiting step of the oxidation. Indeed, in such an electrochemical system, ion transfer is coupled to electron transfer. In other words, anion uptake limits the kinetics and induces a progressive nucleation process. The film acquires an open structure at the end of the oxidation process. On the other hand, during reduction, anion release takes place. An instantaneous nucleation process is observed because the film has previously an open structure. Furthermore, if we compare the rate constants, k_{G-red}^{open*} and k_{G-ox}^{open*}, one observes that the reduction process is much faster that the oxidation (see Figures 5 and 9). The same trend is observed for the compact structure, for instance if we compare k_{G-ox}^{comp*} versus k_{G-red}^{comp*} (see Figures 6 and 10).

We now turn to the interpretation of the redox switching mechanisms in EmiTFSI. On the basis of the chronoamperometry data, both the oxidation and the reduction follow $(ING)_o$-$(ING)_c$ mechanisms. We have shown previously that cation exchange occurred during the redox switching of PEDOT in EmiTFSI.[60] Furthermore, $TFSI^-$ anions are trapped in the polymer matrix and act as plasticizers.[61] Thus, the release of cation during the oxidation that induces a decrease in the film volume follows instantaneous mechanisms. It is well-known that the ionic liquid consists only of Emi^+ cations and $TFSI^-$ anions. This property induces particular properties as compared to classical electrolyte solutions. Indeed, despite the exchange of cation during the redox switching, the polymer remains in an open state because ions are trapped within the film. This behavior explains why the instantaneous mechanisms take place for both the oxidation and the reduction processes. These results indicate that the charge transport mechanism during the redox switching is governed mainly by the physicochemical properties of the medium. In other words, the chemical environment determines the main path for the redox process.

At this stage, it is interesting to analyze the influence of the applied potential E_{app} on the growth rate constants, k_{G-red}^{open*} and k_{G-ox}^{open*}. As shown in Figures 9 and 17, k_{G-red}^{open*} does not vary notably with E_{app} in the two media, whereas k_{G-ox}^{open*} increases with E_{app} (see Figures 5 and 17). Indeed, according to the mechanisms depicted in Scheme 1, the growth rate constants k_{G-red}^{open*} and k_{G-ox}^{open*} depend on the bimolecular rate constant (see eqs 7, 27, or 31) and the fraction X_0 of the polymer involved in the nucleation process (see eq 4). Here, we may assume that the bimolecular rate constant characterizing a self-exchange electron transfer does not vary notably with the applied potential (in turn, with the interfacial electric field). However, the initial fraction of the polymer, X_0, involved the nucleation process may vary with E_{app}. According to these hypotheses, the dependence of k_{G-red}^{open*} and k_{G-ox}^{open*} on the applied potential is mainly due to the variation of X_0.

We now move to the charge storage properties of the conducting polymer. The linear variation of both Q_{ox,t_∞}^{open} and Q_{red,t_∞}^{open}, in NBu_4PF_6 + ACN (Figures 5 and 9) and EmiTFSI (Figures 15 and 16), indicates the capacitive behavior of the system under consideration.[50,57,58] Because the redox responses of PEDOT, and generally for conducting polymers, are related to the intercalation/deintercalation mechanisms, the charge storage properties can be characterized by the chemical capacitance. Indeed, in the light of solid-state electrochemistry, the conducting polymer-modified electrode can be considered as a mixed conductor, because of the electroneutrality condition. A few years ago, Jamnik and Maier indicated that two kinds of capacitance, the electrical and the chemical capacitance, might be involved in charge transport in mixed conductors (electronically and ionically conducting sample).[62,63] In contrast to an electrostatic capacitor, there is no separation of electric charge in a chemical capacitor. The chemical capacitance C_i is directly proportional to the number of carriers within the sample. Then, the larger C_i, the greater is the uptake or release of additional carriers upon a given change of chemical potential μ_i. In other words, the chemical capacitance reflects the capability of the system to accept or release additional charge carriers of type i for a given variation of their chemical potential μ_i. For intercalation materials, the change of Gibbs energy, ΔG, is

related to the variation of the chemical potential. In contrast to the electrostatic capacitance, the chemical capacitance C_i is proportional to the sample volume. The chemical capacitance is defined as the differential of the charge passed with respect to the electrode potential[64]

$$C_i = \frac{dQ}{dV} \tag{39}$$

Moreover, intercalant species being introduced (or released) in the host can cause conformational change of the polymer and leads to internal stress. Then, the change in energy of the host itself can be interpreted as the interaction of the intercalant species with the host. Thus, the chemical capacitance is a feature parameter of the conducting polymer in a given chemical environment, which is independent of the driving force in the linear regime. It should be noted that the concept of chemical capacitance was successfully used to analyze the electrochemical behavior of nanostructured nanocrystalline inorganic semiconducting materials such as TiO_2 in the context of photovoltaic applications.[65−67]

6. Conclusions

The electrochemical responses of PEDOT in NBu_4PF_6 + ACN and a RTIL EmiTFSI were studied within a phenomenological model in which the redox switching is analyzed in terms of the nucleation and growth processes. Results indicate that the electrodeposited film contains two types of coexisting zones: compact and open structures. We show that the physicochemical interaction between the PEDOT film and the medium (solvent and ions) plays an important role and determines the mechanisms. In EmiTFSI, redox switching follows INGs in both oxidation and reduction. However, in NBu_4PF_6 + ACN, PNGs are observed in the oxidation, whereas INGs are found for the reduction. We have pointed out that the initial state of the polymer film (open or compact) determines the progressive or instantaneous nature of the nucleation process. The proposed model allows rationalization of the influence of the chemical environment on the redox switching dynamics of PEDOT and conducting polymers in general. Thus, the model may be useful for the development of electrochemical devices based on conducting polymers, such as electrochemical actuators and electrochromic systems. Work is in progress to correlate the charge transfer dynamics and the mechanical properties of the film.

Acknowledgment. This work was supported by the French Ministry of Research, the CNRS, and the Agence Nationale pour la Recherche (Grants ANR-06-BLAN-0296). We are particularly grateful to Dr. J. S. Lomas (ITODYS, University Paris 7), who kindly revised our text and helped us to put it into correct English.

Supporting Information Available: Figures showing the variation of the ratio of the charge corresponding the open state with respect to the total charge for both oxidation and reduction processes, in ACN and ionic liquid. This material is available free of charge via the Internet at http://pubs.acs.org.

References and Notes

(1) Nalwa, H. S. *Handbook of Organic Conductive Molecules and Polymers*; John Wiley & Sons: Chichester, England, 1997; Vols. 1−4.
(2) Skotheim, T. A.; Elsenbaumer, R. L.; Reynolds, J. R. *Handbook of Conducting Polymers*, 2nd ed.; Marcel Dekker: New York, 1998.
(3) Inzelt, G.; Pineri, M.; Schultze, J. W.; Vorotyntsev, M. A. *Electrochim. Acta* **2000**, *45*, 2403.
(4) Hegger, A. J. *J. Phys. Chem. B* **2001**, *105*, 8475.
(5) MacDiarmid, A. G. *Synth. Met.* **2002**, *125*, 11.
(6) Lyons, M. E. G., Ed.; *Electroactive Polymer Electrochemistry*; Plenum Press: New York, 1994; Vol. 1.
(7) Hillman, A. R.; Bruckenstein, S. *J. Chem. Soc. Faraday Trans.* **1993**, *89*, 339.
(8) Hillman, A. R.; Bruckenstein, S. *J. Chem. Soc. Faraday Trans.* **1992**, *89*, 3779.
(9) Kalaji, M.; Peter, L. M.; Abrantes, L. M.; Mesquita, J. C. *J. Electroanal. Chem.* **1989**, *274*, 289.
(10) Kalaji, M.; Nyholm, L.; Peter, L. M. *J. Electroanal. Chem.* **1992**, *325*, 269.
(11) Vuki, M.; Kalaji, M.; Nyholm, L.; Peter, L. M. *J. Electroanal. Chem.* **1992**, *332*, 315.
(12) Otero, T. F.; Grande, H. J.; Rodriguez, J. *J. Phys. Chem. B* **1997**, *101*, 3688.
(13) Otero, T. F.; Grande, H. J.; Rodriguez, J. *J. Phys. Chem. B* **1997**, *101*, 8525.
(14) Grande, H. J.; Otero, T. F. *Electrochim. Acta* **1999**, *44*, 1893.
(15) Levi, M. D.; Lopez, C.; Vieil, E.; Vorotyntsev, M. A. *Electrochim. Acta* **1997**, *42*, 757.
(16) Vorotyntsev, M. A.; Vieil, E.; Heinze, J. *J. Electroanal. Chem.* **1998**, *450*, 121.
(17) Pei, Q.; Inganäs, O. *J. Phys. Chem.* **1993**, *97*, 6034.
(18) Chen, X.; Xing, K.-Z.; Inganäs, O. *Chem. Mater.* **1996**, *8*, 2439.
(19) Rodriguez Presa, M. J.; Posadas, D.; Florit, M. I. *J. Electroanal. Chem.* **2000**, *482*, 117.
(20) Odin, C.; Nechtschein, M. *Phys. Rev. Lett.* **1991**, *67*, 1114.
(21) Odin, C.; Nechtschein, M. *Synth. Met.* **1991**, *44*, 177.
(22) Odin, C.; Nechtschein, M. *Synth. Met.* **1992**, *47*, 329.
(23) Odin, C.; Nechtschein, M.; Hapiot, P. *Synth. Met.* **1992**, *47*, 329.
(24) Aoki, K.; Cao, J.; Hoshino, Y. *Electrochim. Acta* **1994**, *39*, 2291.
(25) Noël, V.; Randriamahazaka, H.; Chevrot, C. *J. Electroanal. Chem.* **2003**, *542*, 33.
(26) Aoki, K. *J. Electroanal. Chem.* **1991**, *310*, 1.
(27) Aoki, K.; Cao, J.; Hoshino, Y. *Electrochim. Acta* **1993**, *38*, 1711.
(28) Aoki, K. *J. Electroanal. Chem.* **1994**, *373*, 67.
(29) Aoki, K.; Kawase, M. *J. Electroanal. Chem.* **1994**, *377*, 125.
(30) Tezuka, Y.; Kimura, T.; Ishii, T.; Aoki, K. *J. Electroanal. Chem.* **1995**, *395*, 51.
(31) Aoki, K.; Edo, T.; Cao, J. *Electrochim. Acta* **1998**, *43*, 285.
(32) Lacroix, J. C.; Diaz, A. F. *J. Electrochem. Soc.* **1988**, *135*, 1457.
(33) Lacroix, J. C.; Diaz, A. F. *Makromol. Chem. Macromol. Symp.* **1987**, *8*, 17.
(34) Lacroix, J. C.; Fraoua, K.; Lacaze, P. C. *J. Electroanal. Chem.* **1998**, *444*, 83.
(35) Miomandre, F.; Bussac, M. N.; Vieil, E.; Zuppiroli, L. *Electrochim. Acta* **1999**, *44*, 2019.
(36) Miomandre, F.; Bussac, M. N.; Vieil, E.; Zuppiroli, L. *Chem. Phys.* **2000**, *255*, 291.
(37) Otero, T. F.; Boyano, I. *J. Phys. Chem. B* **2003**, *107*, 6730.
(38) Wang, X.; Smela, E. *J. Phys. Chem. C* **2009**, *113*, 369.
(39) Wang, X.; Shapiro, B.; Smela, E. *J. Phys. Chem. C* **2009**, *113*, 382.
(40) West, B. J.; Otero, T. F.; Shapiro, B.; Smela, E. *J. Phys. Chem. B* **2009**, *113*, 1277.
(41) Otero, T. F.; Boyano, I. *J. Phys. Chem. B* **2003**, *107*, 4269.
(42) Randriamahazaka, H.; Vidal, F.; Dassonville, P.; Chevrot, C.; Teyssié, D. *Synth. Met.* **2002**, *128*, 197.
(43) Hillman, A. R.; Daisley, S. J.; Bruckenstein, S. *Electrochem. Commun.* **2007**, *9*, 1316.
(44) Hillman, A. R.; Daisley, S. J.; Bruckenstein, S. *Electrochim. Acta* **2008**, *53*, 3763.
(45) Hillman, A. R.; Mohamoud, M. A.; Bruckenstein, S. *Electroanalysis* **2005**, *17*, 1421.
(46) Pater, E.; Bruckenstein, S.; Hillman, A. R. *J. Phys. Chem. B* **2006**, *110*, 14761.
(47) Onishi, K.; Sewa, S.; Asaka, K.; Fujiwara, N.; Oguro, K. *Electrochim. Acta* **2001**, *46*, 1233.
(48) Sugino, T.; Kiyohara, K.; Takeuchi, I.; Mukai, K.; Asaka, K. *Sens. Actuators, B* **2009**, *141*, 179.
(49) Groenendaal, L.; Jonas, F.; Freitag, D.; Pielartzik, H.; Reynolds, J. R. *Adv. Mater.* **2000**, *12*, 481.
(50) Randriamahazaka, H.; Plesse, C.; Teyssié, D.; Chevrot, C. *Electrochem. Commun.* **2003**, *5*, 613.
(51) Otero, T. F. *J. Mater. Chem.* **2009**, *19*, 681.
(52) Wang, X.; Smela, E. *J. Phys. Chem. C* **2009**, *113*, 359.
(53) Philipp, R.; Dittrich, J.; Retter, U.; Müller, E. *J. Electroanal. Chem.* **1988**, *250*, 159.
(54) Avrami, M. *J. Chem. Phys.* **1939**, *7*, 1103.

(55) Bonhôte, P.; Dias, A.-P.; Papageorgious, N.; Kalyanasundaram, K.; Grätzel, M. *Inorg. Chem.* **1996**, *35*, 1168.

(56) Randriamahazaka, H.; Noel, V.; Chevrot, C. *J. Electroanal. Chem.* **1999**, *472*, 103. Erratum: **1999**, *476*, 183.

(57) Randriamahazaka, H.; Plesse, C.; Teyssié, D.; Chevrot, C. *Electrochim. Acta* **2005**, *50*, 1515.

(58) Randriamahazaka, H.; Plesse, C.; Teyssié, D.; Chevrot, C. *Electrochim. Acta* **2005**, *50*, 4222.

(59) Randriamahazaka, H.; Noël, V.; Chevrot, C. *J. Electroanal. Chem.* **2004**, *556*, 35.

(60) Randriamahazaka, H.; Plesse, C.; Teyssié, D.; Chevrot, C. *Electrochem. Commun.* **2004**, *6*, 299.

(61) Randriamahazaka, H.; Plesse, C.; Vidal, F.; Gautier, C.; Chevrot, C.; Teyssié, D. *Proc. SPIE* **2004**, *5385*, 294.

(62) Jamnik, J.; Maier, J. *J. Electrochem. Soc.* **1999**, *146*, 4183.

(63) Jamnik, J.; Maier, J. *Phys. Chem. Chem. Phys.* **2001**, *3*, 1668.

(64) Bisquert, J. *Electrochim. Acta* **2002**, *47*, 2435.

(65) Bisquert, J. *Phys. Chem. Chem. Phys.* **2003**, *5*, 5360.

(66) Fabregat-Santiago, F.; Randriamahazaka, H.; Zaban, A.; Garcia-Canadas, J.; Garcia-Belmonte, G.; Bisquert, J. *Phys. Chem. Chem. Phys.* **2006**, *8*, 1827.

(67) Bisquert, J.; Fabregat-Santiago, F.; Mora-Sero, I.; Garcia-Belmonte, G.; Barea, E. M.; Palomares, E. *Inorg. Chim. Acta* **2008**, *361*, 684.

JP1094432